Fingertip Force Control with Embedded Fiber Bragg Grating Sensors

Yong-Lae Park[1], Seok Chang Ryu[1], Richard J. Black[2], Behzad Moslehi[2], and Mark R. Cutkosky[1]

[1]Center for Design Research, Stanford University
Stanford, CA 94305-2232, USA
{ylpark, scryu, cutkosky}@stanford.edu

[2]Intelligent Fiber Optic Systems Corporation (http://www.ifos.com)
2363 Calle Del Mundo, Santa Clara, CA 95054, USA
{rjb, bm}@ifos.com

Abstract— We describe the dynamic testing and control results obtained with an exoskeletal robot finger with embedded fiber optical sensors. The finger is inspired by the designs of arthropod limbs, with integral strain sensilla concentrated near the joints. The use of fiber Bragg gratings (FBGs) allows for embedded sensors with high strain sensitivity and immunity to electromagnetic interference. The embedded sensors are useful for contact detection and for control of forces during fine manipulation. The application to force control requires precise and high-bandwidth measurement of contact forces. We present a nonlinear force control approach that combines signals from an optical interrogator and conventional joint angle sensors to achieve accurate tracking of desired contact forces.

I. INTRODUCTION

In several applications, optical fiber sensors have been utilized as an alternative to piezoresistive sensors for robot force sensing and control. The most common uses have been for tactile sensing, where the robustness of optical fibers and the ability to process the information with a CCD or CMOS camera are advantageous [8], [12], [16]. Other applications include using optical fibers in which the loss of light is a function of the bending curvature to measure the bending of the fingers of a glove [11] or other flexible structure [7]. More recently, FBG sensors have been used as precise optical strain gages for structures [18], [24]. The FBG sensors produce shifts in the wavelength of reflected light as a local region of the fiber experiences axial strain. Very small strains, on the order of 0.1 μstrain, can be resolved. In comparison to conventional strain gages, this sensitivity allows the sensors to be used in sturdy structures that experience small stresses and strains under normal loading conditions.

All of these sensor developments can take advantage of the electromagnetic noise immunity of optical sensors. As a consequence, they are ideally suited for use around industrial robots with large motors under pulse-width modulated control, in space applications and even in magnetic resonance imaging (MRI) machines. In addition, as demonstrated by Ascari et al. [1], optical communication can be used to provide a high-bandwidth pathway for taking tactile and force information down the robot arm, using only a single optical fiber. For the case of FBG sensors, it is additionally possible
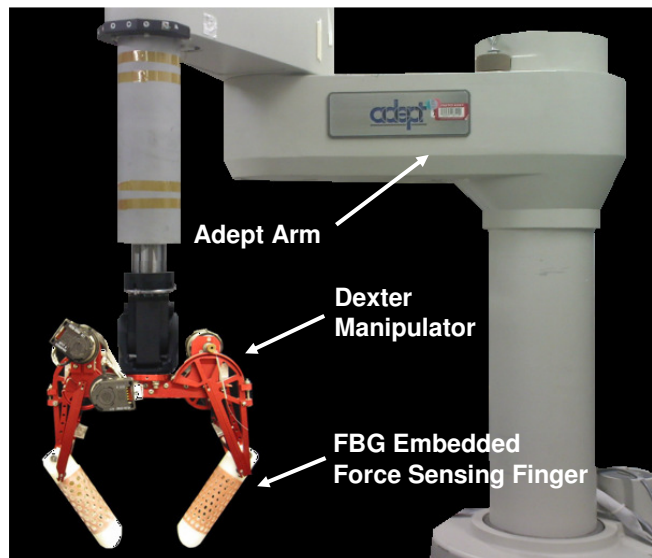

Fig. 1. FBG embedded force sensing finger prototypes integrated with Dexter [9] manipulator and Adept robot arm

to multiplex optically, putting several sensors along a single fiber and interrogating them with different wavelengths of light.

In a previous paper [18] we reported on the design and fabrication process for creating a lightweight, hollow robotic finger with embedded FBG sensors. We also showed that by placing a small number of FBG strain sensors near a joint, in a design inspired by arthropod exoskeletons [2], [5], we could resolve contact locations using intrinsic tactile sensing [3], [4]. In the present paper, we extend this work to address dynamic characterization of the sensorized finger structures and demonstrate their application in closed-loop force control. Because the structures are made of polymers, they are subject to a certain amount of creep and hysteresis. However, by embedding a reinforcing mesh, these effects are reduced and can easily be accommodated in a force control scheme.

Figure 1 shows the integrated robot system for the control experiments. We describe the force controller that we have

implemented for the finger and demonstrate that precise control of manipulation forces is possible when a hand equipped with such optical sensors is mounted on a large industrial robot that produces considerable electromagnetic noise. We also describe ongoing work to miniaturize the technology so that multiple FBG sensors can be applied to human-scale robotic fingertips or tools for minimally invasive surgery. At this scale, optical multiplexing is particularly desirable to eliminate bundles of wires that must be routed down the fingers and arm.

II. DYNAMIC SENSOR CHARACTERIZATION

A. Modes of Vibration

Prior to setting up a closed-loop control system, we investigated the dynamic response of the sensorized fingers. Figure 2 shows the impulse (expressed as a change in the wavelength of light reflected by an FBG cell) and its fast Fourier transform (FFT). The impulse was effected by tapping on the finger with a light and stiff object. The FFT shows a dominant frequency around 167 Hz which is a result of the dominant vibration mode.

A finite element analysis (Figure 3) indicates that the dominant modes correspond to bending about the orthogonal X and Y axes, with nearly equal predicted frequencies of just over 180 Hz. The difference between the computed and measured frequency is due mainly to imperfect modeling of the local stiffness of the polymer/mesh composite, which depends on manufacturing tolerances and especially on the actual location of the mesh fibers within the polymer structure. (A description of the construction of the structure is given in [18].)
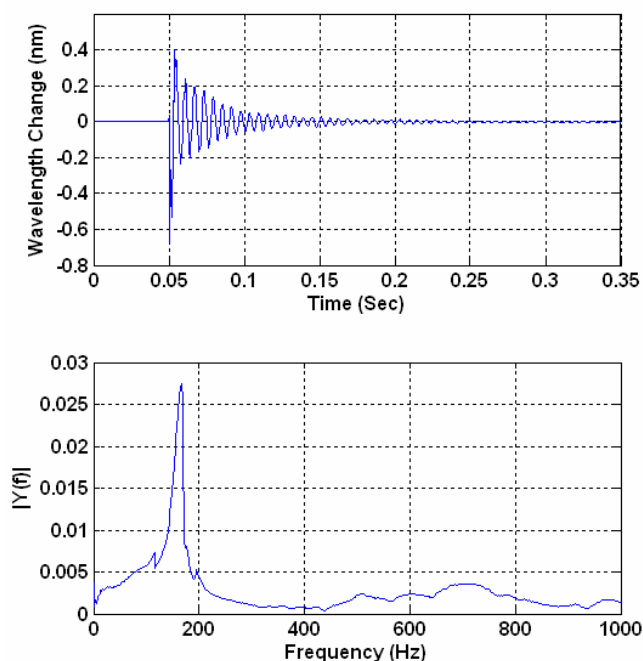
Mode	1	2	3	4	5
Frequency	181.2 Hz	185.1 Hz	479.1 Hz	938.7 Hz	941.5 Hz

Fig. 3. Modes of vibration of the finger prototype using finite element analysis (Modes 1 and 2 represent bending in X and Y axes respectively.)

B. Hysteresis Analysis

Polymer structures in general are subject to a certain amount of creep and hysteresis, which is one reason why they have traditionally been avoided for force sensing and control applications. In the present case, these effects are mitigated by embedding a copper mesh within the structure.

However, there is still some creep and hysteresis as shown in Figures 4 and 5. The plot in Figure 4 was produced by applying a moderate load of approximately 1.8 N to the finger for several seconds and then removing it suddenly. Figure 5 shows detailed views of loading and unloading periods. The measured force is obtained by optically interrogating the calibrated FBG sensors.

When a steady load is applied for several seconds there is a small amount of creep, part of which also arises from imperfect thermal compensation in the polymer structure. The effect is relatively small over periods of a few seconds, corresponding to typical grasping durations in a pick-and-place or manipulation task. A more significant effect occurs when the load is released. As the plots indicate, the force quickly drops to a value of approximately 0.1 N and then more slowly approaches zero. To overcome this effect in manipulation tasks a simple strategy was employed. Whenever the force suddenly drops to a small value (less than 0.17 N), we assume that contact has been broken and that the force is actually zero. At this point we reset the zero-offset after a brief time delay. As described in the following section, the

Fig. 2. Impulse response (top) of the finger prototype and its fast Fourier transform (bottom)
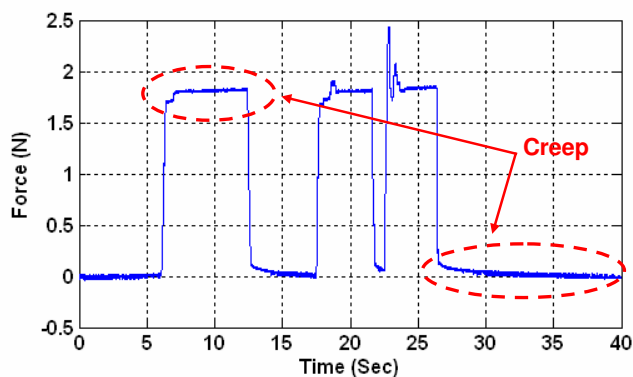

Fig. 4. Testing the effect of applying a steady load for several seconds and suddenly removing it from the polymer fingertip (Figure 5 shows detailed views of typical loading and unloading periods.)
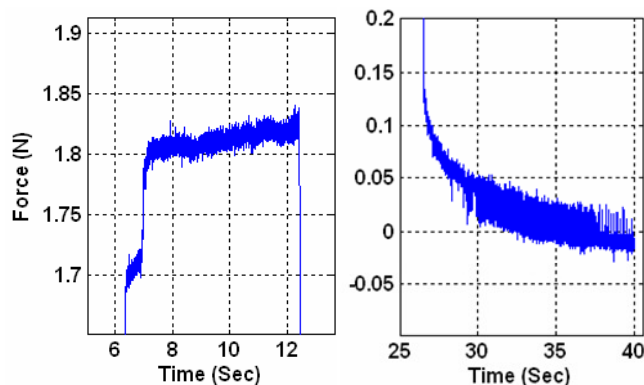
Fig. 5. Detailed views of the creep under steady loading (left) and of the hysteresis associated with sudden unloading (right)

loss of contact is also a signal to switch the hand from force control to position control.

III. CONTROL SYSTEM DESCRIPTION

A. Hardware Description

Figure 6 shows the overall architecture of the components and hardware system. The two-fingered robot hand, Dexter, is a low-friction, low-inertia device designed for accurate force control. The hand is controlled by a process running under a real-time operating system (QNX) at 1000 Hz, which reads the joint encoders, computes kinematic and dynamic terms and produces voltages for linear current amplifiers that drive the motors.

A more complete description of the hand is provided in [9]. The hand controller also acquires force information, via shared memory, from a process that obtains analog force information at 5 kHz from the IFOS' I-Sense[TM] optical interrogator that monitors the fiber optic sensors.

The optical interrogator is based on high-speed parallel processing Wavelength Division Multiplexing (WDM). Multiple FBG sensors are addressed by spectral slicing, with the available source spectrum divided up so that each sensor is addressed by a different part of the spectrum. The interrogator built for this work uses 16 channels of a parallel optical processing chip with each channel separated by 100 GHz (approximately 0.8 nm wavelength spacing around an operating wavelength of 1550 nm [1]) so that the total required source bandwidth is 12.8 nm. We describe how this approach can be adapted to support larger numbers of FBG sensors on a single fiber in Appendix.

The Dexter hand is mounted to a commercial AdeptOne-MV 5-axis industrial robot. Communication with the Adept robot is performed using the ALTER software package, which allows new positions to be sent to the robot over an Ethernet connection every 16 ms (62.5 Hz). Due to this limitation, all force control is done within the Dexter hand, and the Adept robot is used only for large motions and to

---

[1]Operation is in the 1550-nm wavelength window (centered around C-band) to exploit the greatest availability and price breaks of components from telecom applications.
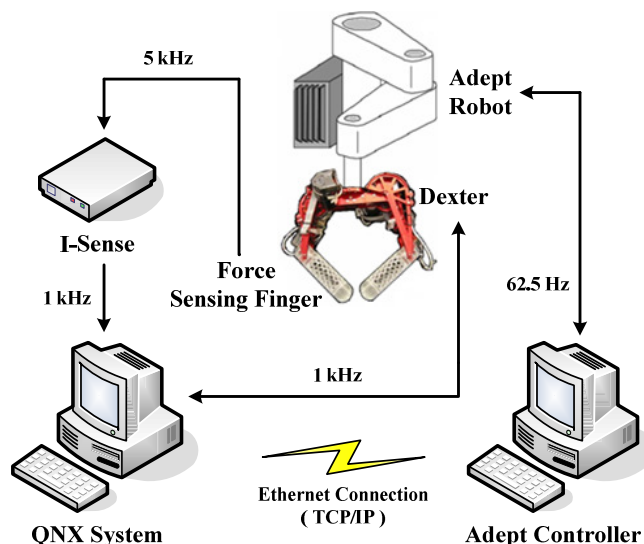

Fig. 6. Overall Hardware System Architecture

keep the Dexter hand approximately centered in the middle of its workspace.

When the fingers are not in contact with an object, they are operated under computed-torque position control, with real-time compensation for gravity torques and inertial terms. When in contact with an object, they are switched over to a nonlinear force control as described in the next section.

B. Software Description

All the internal processes are carried out in the QNX OS in real-time. Figure 7 depicts the overall internal process architecture to control different components independently but simultaneously. The figure shows how different processes perform their tasks interacting with other processes in real time. The Driver process calls each sub-process whenever it is needed. The User input process obtains user inputs for the configuration of the system. The configuration data are stored in Shared Memory. The Adept control process continuously
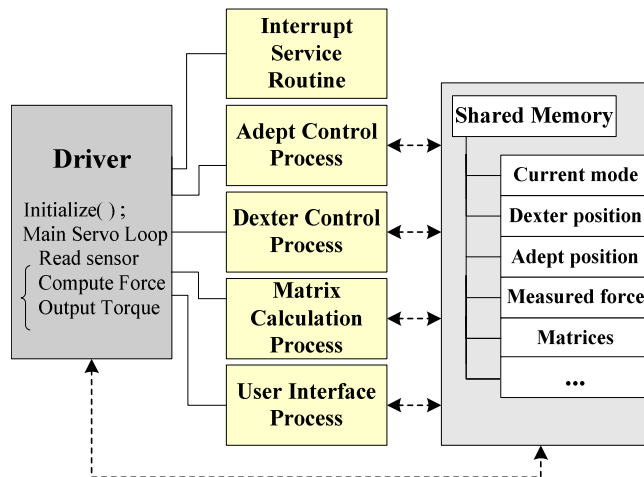

Fig. 7. Overall Internal Process Architecture

feeds the next position and orientation (X, Y, Z, Rx, Ry, Rz) every 16 ms.

IV. CONTACT FORCE CONTROL

Most applications of contact force control can be divided into two main categories: impedance control and force control [23]. The impedance control [10], [13] aims at controlling position and force by establishing desired contact dynamics while the force control [19] commands the system to track a force set-point directly. For this work we adopted a class of nonlinear controller presented by our collaborator H. Seraji [20], [21], [22]. When the system detects contact with the fingertip, it switches to force control as depicted in Figure 8. The system actually performs hybrid force/position control [14], [19] at this stage in that both position and force controllers are combined to control forces. The proportional-integral (PI) force controller is constructed as

$$K(s) = k_p + \frac{k_i}{s}$$

based on the first-order admittance

$$Y(s) = k_p s + k_i$$

where k_p and k_i are the proportional and integral force feedback gains respectively. To make the controller simple, we fix the proportional gain k_p to a constant and make the integral gain k_i a nonlinear function of the force error. The nonlinear integral gain is determined by the sigmoidal function

$$k_i = k_0 + \frac{k_1}{1 + \exp[-\text{sgn}(\Delta)k_2 e]}$$

where e is the force error ($F_r - F$), $\Delta = F_r - F_s$, F_s is the steady value of the contact force and k_0, k_1, and k_2 are user-specified positive constants which determine the minimum value, the range of variation, and the rate of variation of k_i respectively. The value of $\text{sgn}(\Delta)$ is +1 when $F_r > F_s$, and -1 when $F_r < F_s$.

We can achieve fast responses and small oscillations in control with this nonlinear gain since the nonlinearity provides high gains with large errors and low gains with small errors. To minimize oscillations due to large proportional gains when the switch occurs between position and force control, all gains except the integral force feedback gain are ramped from zero to the defined values over a transition time of 0.1 second.
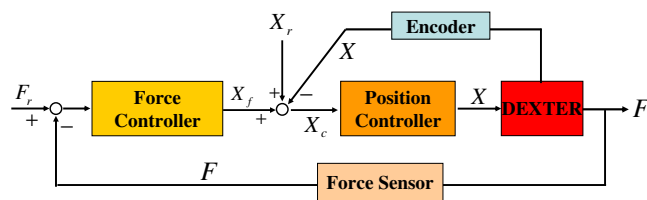

Fig. 8. Position based smart force control system where F and F_r are contact force and user-specified force setpoint, and X, X_c, X_f, and X_r are actual position, commanded position, positioin perturbation computed by the force controller, and reference position of the end effector respectively

A. Results of Experiments

In this section we present the results of two experiments that assess the accuracy of control achieved with the finger prototype. The first experiment shows how accurately the manipulator maintains a desired force during a contact by comparing the force data from the prototype with that from a commercial 6-axis force-torque sensor (ATI-Nano25 from ATI Industrial Automation). The second experiment shows the force control during manipulation tasks including linear and rotational motions of the hand while grasping an object.

1) Experiment 1 (Force Setpoint Tracking): The Adept arm moves in one direction until the fingertip touches an object, which happens to be a commercial load cell. As soon as the finger detects contact, the Adept stops and the Dexter hand switches to force control. After a period of time the Adept moves away from the object and the hand switches back to position control. Figure 9 shows the horizontal motion of the Adept arm in parallel with the joint rotation of the distal joint of the Dexter hand and the force
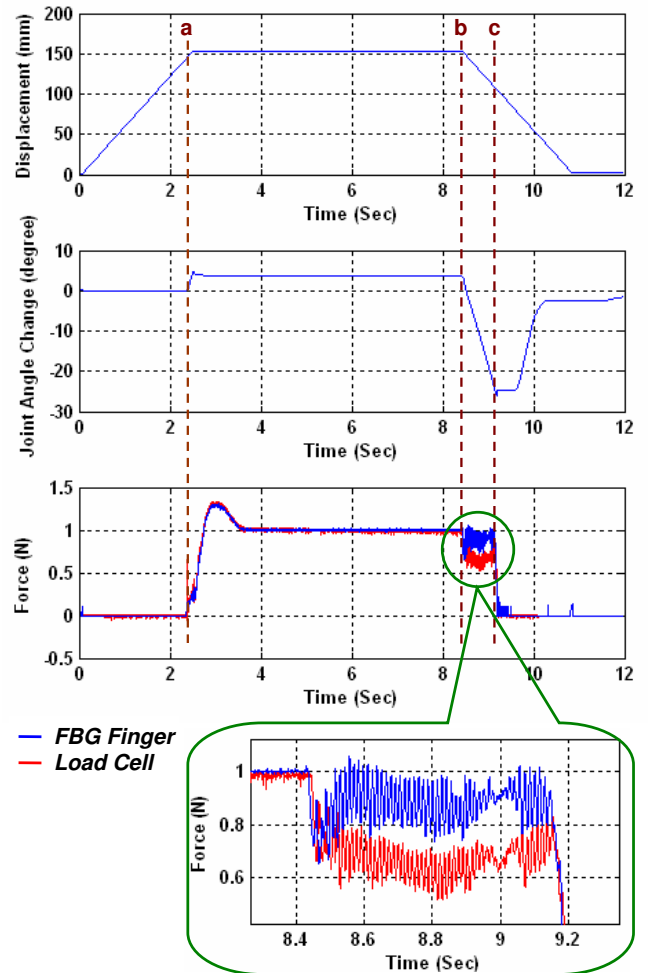

Fig. 9. Adept robot motion (top), joint angle change of Dexter manipulator (middle), and force data from load cell and FBG embedded robot finger prototype (bottom); The robot starts force control as soon as it makes a contact to the object (a). After a certain period of time the robot starts to retreat (b), and finally breaks contact (c).

data from the fingertip and the commercial load cell. The result shows the two sets of force data almost exactly match over the several seconds of the experiment. As the finger breaks contact, there is a small amount of slippage reflected in the mirror-image dynamic force signals reported by the finger and load cell, respectively.

We note also that to produce this plot it was necessary to carefully shield and ground all wires emanating from the commercial load cell due to the large magnetic fields produced by the industrial robot.

2) Experiment 2 (Force Control during Manipulation): Experiment 2 concerns the ability of the hand to maintain a desired grasp force while subject to motions in a manipulation task. For the results shown in Figure 10, the robot was commanded to lift the grasped object weighing 100 grams, move it horizontally a distance of approximately 30 cm, rotate it about the Z and Y axes, return to the original location, and replace the object. The magnitude of combined (x, y, and z) acceleration of the manipulator is plotted in parallel with the measured grasp force. Disturbances associated with the accelerations and decelerations along the path can be observed in the force data. However, in every case the controller returns to the desired force within 0.01 seconds, and the root-mean-square of force errors during the force control is < 0.03 N.

Since the current finger prototype is capable of measuring three-axis forces, more complicated force control experiments in two or three axes will be carried out in the future.

V. Conclusions and Future Work

We have presented the application of robotic fingers with four embedded FBG sensors for force control in a robot hand. The fingers are made in the form of a hollow shell with a hexagonal grid pattern for strength and light weight. The material is a urethane polymer with embedded optical fibers and an embedded copper mesh to reduce creep and provide some thermal shielding. Although any such polymer composite structure will exhibit more hysteresis than a machined metal part, we demonstrate in the experiments that the effects are small over short periods of a few seconds or less and do not compromise the ability of the hand to maintain control of the grasp force during manipulation tasks.

The hand is operated in a hybrid control scheme that switches between computed-torque position control and non-linear force control when contact is sensed. The finger sensors are capable of resolving small forces and are immune to electromagnetic disturbances so that the system can be mounted on a large industrial robot, or in other applications where large magnetic fields are present, without concern for shielding and grounding. In addition, as multiple FBG sensors can be placed along a single fiber and multiplexed optically, it suffices to route a single optical fiber down the robot arm.

The next steps are to miniaturize the technology and provide larger numbers of sensors on a structure. The motivation is to produce human-scale robotic fingertips for robots designed for human interaction in space applications and to produce sensorized end-effectors suitable for robot-assisted minimally invasive surgery. By using versions of fingertips with no metal components, manipulation applications within MRI devices could also be addressed.

Figure 11 shows a prototype of a small fingertip with an embedded optical fiber containing FBG strain sensors. For this application, an 80-μm diameter bend-resistant optical fiber from OFS was selected. These fibers tolerate comparatively tight bending radii of approximately 7.5 mm. Tests on the new fingertip are underway.

In parallel, we are adapting the optical fiber interrogator [6], [15], [17] to support larger numbers of sensors - see Appendix for practical sensor numbers. In our parallel pro-
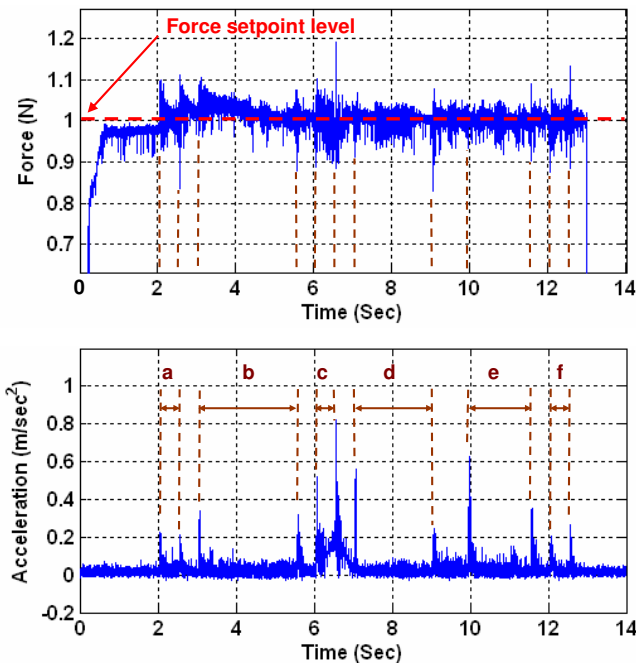

Fig. 10. Grasp force measured by a finger with FBG sensors during a manipulation task (top) plotted along with magnitude of combined (x, y, and z) acceleration of the robot (bottom); periods a, b, e, and d are for translation motions, and periods c and d for rotation motions. (Every task motion is followed by a waiting period before starting next motions.)
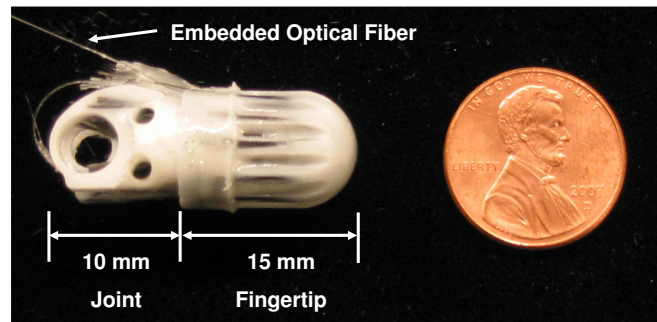

Fig. 11. Miniaturized polyurethane finger prototype fabricated as a hollow shell composed of several curved ribs that are connected at the base by a circular ring and meet at the apex. One optical fiber with four FBG sensors is embedded in the ribs.

cessing architecture using a broad-band source, the speed is mainly limited by the electronics and the required resolution. This is in contrast to interrogators based on tunable sources or filters where the tuning speed provides the limitation. We are developing electronics to support more wavelength channels and use a larger portion of the available source spectrum, enabling more sensors to be addressed.

APPENDIX

For the range of broadband light sources that we use, the available source bandwidth is between 40 nm and 100 nm. Thus, if we make use of the entire available source spectrum, we can support 20-50 sensors on a single fiber. This number can be increased by using multiple fibers. In particular, the number of sensors $N_{sensors}$ that can be supported on a single fiber is related to the source bandwidth $\delta\lambda_{source}$ divided by the bandwidth required for each sensor $\delta\lambda_{sensor}$. Further $\delta\lambda_{sensor}$ is given by the maximum strain-dependent wavelength shift $\delta\lambda_{\mathrm{strain-max}}$ and the sensor wavelength separation to avoid crosstalk (i.e., to keep it below a "tolerable" level, $\delta\lambda_{cross-talk}$). Thus,

$$N_{sensors} = \frac{\delta\lambda_{source}}{\delta\lambda_{\mathrm{strain-max}} + \delta\lambda_{cross-talk}}.$$

The wavelength separation to avoid crosstalk will depend on both the FBG spectrum and the parallel spectral processor, but is typically on the order of wavelength channel separation, 0.8 nm. Table I summarizes the possible numbers of sensors for different source bandwidths and maximum strain-dependent wavelength shifts assuming $\delta\lambda_{cross-talk} = 0.8$ nm.

TABLE I

TYPICAL SENSOR NUMBERS THAT CAN BE SUPPORTED FOR A RANGE OF SPECTRAL CHARACTERISTICS AND STRAIN REQUIREMENTS

$\delta\lambda_{source}$	$\delta\lambda_{\mathrm{strain-max}}$	$N_{sensors}$
100 nm	1.2 nm ($\rightarrow$1200 μstrain)	50
	9.2 nm ($\rightarrow$9200 μstrain)	10
40 nm	1.2 nm	20
	9.2 nm	4

REFERENCES

[1] L. Ascari, P. Corradi, L. Beccai, and Laschi. A miniaturized and flexible optoelectronic sensing system for a tactile skin. *International Journal of Micromechanics and Microengineering*, 17:2288–2298, 2007.

[2] F. G. Barth and J. Stagl. The slit sense organs of arachnids. *Zoomorphologie*, 86:1–23, 1976.

[3] A. Bicchi, J. K. Salisbury, and D. L. Brock. Contact sensing from force measurements. *International Journal of Robotics Research*, 12(3):249–262, 1993.

[4] A. Bicchi, J. K. Salisbury, and P. Dario. Augmentation of grasp robustness using intrinsic tactile sensing. *Proceedings of the 1989 IEEE International Conference on Robotics and Automation*, 1:302–307, 1989.

[5] R. Blickhan and F. G. Barth. Strains in the exoskeleton of spiders. *Journals of Comparative Physiology A*, 157:115–147, 1985.

[6] K. Chau, P. Qiao, W. Lestari, R. J. Black, and B. Moslehi. High-speed, high-resolution fiber Bragg grating matrix structural health monitoring systems. *Proceedings of the SPIE Sensor Systems and Networks: Phenomena, Techonology, and Applications for NDE and Health Monitoring*, 6530(1):Q1–Q12, 2007.

[7] L. A. Danisch, K. Englehart, and A. Trivett. Spatially continuous six degree of freedom position and orientation sensor. *Sensor Review*, 19(2):106–112, 1999.

[8] L. A. Danisch and E. M. Reimer. World patent of canadian space agency. pages PCT, Wo. 99, No.04234, 1999.

[9] W. Griffin, W. M. Provancher, and M. R. Cutkosky. Feedback strategies for telemanipulation with shared control of object handling forces. *Presence: Teleoperations and Virtual Environments, MIT Press*, 14(6):720–731, 2005.

[10] N. Hogan. Impedence control: An approach to manipulation, parts i-iii. *ASME Journal of Dynamic Systems, Measurement, and Control*, 107(1):1–24, 1985.

[11] J. Hong and X. Tan. Calibrating a VPL dataglove for teleoperating the utah/mit hand. *Proceedings of the 1989 IEEE International Conference on Robotics and Automation*, 3:1752–1757, 1989.

[12] K. Kamiyama, H. Kajimoto, M. Inami, N. Kawakami, and S. Tachi. Development of a vision-based tactile sensor. *IEEJ Transactions on Sensors and Micromachines*, 123(1):16–22, 2003.

[13] H. Kazernooni, T. B. Sheridan, and P. K. Houpt. Robust compliant motion for manipulators, parts i-ii. *IEEE Transaction of Robotics and Automation*, RA-2(2):83–105, 1986.

[14] G. Liu and Z. Li. A unified geometric approach to modeling and control of constrained mechanical systems. *IEEE Transactions on Robotics and Automation*, 18(4):574–587, 2002.

[15] C. Lopatin, E. Mendez, B. Moslehi, R. J. Black, K. Chau, and L. Oblea. Progress in miniaturization of a multichannel optical fiber Bragg grating sensor interrogator. *Proceedings of SPIE Third European Workshop on Optical Fibre Sensors*, 6619, 2007.

[16] H. Maekawa, K. Tanie, and K. Komoriya. Tactile feedback for multifingered dynamic grasping. *IEEE Control Systems Magazine*, 17(1):63–71, 1997.

[17] B. Moslehi, R. J. Black, K. Toyama, and H. J. Shaw. Multiplexible fiber-optic strain sensor system with temperature compensation capability. *Divisions 1-3*, U.S. Patents 6,895,132, (issued May 17, 2005), 6,788,835, issued Sept 7, 2004, 6,597,822 (issued July 22, 2003).

[18] Y-L. Park, K. Chau, R. J. Black, and M. R. Cutkosky. Force sensing robot fingers using embedded fiber Bragg grating sensors and shape deposition manufacturing. *Proceedings of the 2007 IEEE International Conference on Robotics and Automation*, pages 1510–1516, 2007.

[19] M. Raibert and J. Craig. Hybrid position/force control of manipulators. *ASME Journal of Dynamic Systems, Measurement, and Control*, 102(2):126–133, 1981.

[20] H. Seraji. A new class of nonlinear PID controllers with robotic applications. *Journal of Robotic Systems*, 15(3):161–181, 1998.

[21] H. Seraji, D. Lim, and R. Steele. Experiments in contact control. *Journal of Robotic Systems*, 13(2):53–73, 1996.

[22] H. Seraji and R. Steele. Nonlinear contact control for space station dexterous arms. *Proceedings of the 1998 IEEE International Conference on Robotics and Automation*, 1:899–906, 1998.

[23] G. Zeng and A. Hemami. An overview of robot force control. *Robotica*, 15:473–482, 1997.

[24] L. Zhang, J. Qian, Y. Zhang, and L. Shen. On SDM/WDM FBG sensor net for shape detection of endoscope. *Proceedings of the 2005 IEEE International Conference on Robotics and Automation*, 4:1986–1991, 2005.